On the discovery of CO nighttime emissions on Titan by Cassini/VIMS: Derived stratospheric abundances and geological implications

Kevin H. Baines[a,*], Pierre Drossart[b], Miguel A. Lopez-Valverde[c], Sushil K. Atreya[d], Christophe Sotin[e], Thomas W. Momary[a], Robert H. Brown[f], Bonnie J. Buratti[a], Roger N. Clark[g], Philip D. Nicholson[h]

[a]*Jet Propulsion Laboratory, California Institute of Technology, M/S 183-601, 4800 Oak Grove Drive, Pasadena, CA 91109, USA*
[b]*LESIA (CNRS-UMR 8109), Observatoire de Paris, Meudon, France*
[c]*Instituto de Astrofisica de Andalucia, Apdo 3004, 18080 Granada, Spain*
[d]*Department of Atmospheric, Oceanic, and Space Sciences, The University of Michigan, Ann Arbor, MI 48109-2143, USA*
[e]*Laboratoire de Planétologie et Géodynamique, UMR-CNRS 6112, Faculté des Sciences, Universite de Nantes, B. P. 92208, 2 Rue de la Houssenière, 44072 Nantes Cedex 03, France*
[f]*Lunar and Planetary Lab and Stewart Observatory, University of Arizona, Tucson, AZ 85721, USA*
[g]*US Geological Survey, M/S 964, Box 25046 Federal Center, Denver, CO 80225, USA*
[h]*Cornell University, Astronomy Department, Space Sciences Bldg., Ithaca, NY 14853, USA*

Abstract

We present a quantitative analysis of CO thermal emissions discovered on the nightside of Titan by Baines et al. [2005. The atmospheres of Saturn and Titan in the near-infrared: First results of Cassini/VIMS. Earth, Moon, and Planets, 96, 119–147]. in Cassini/VIMS spectral imagery. We identify these emission features as the P and R branches of the 1-0 vibrational band of carbon monoxide (CO) near 4.65 μm. For CH_3D, the prominent Q branch of the v_2 fundamental band of CH_3D near 4.55 μm is apparent. CO_2 emissions from the strong v_3 vibrational band are virtually absent, indicating a CO_2 abundance several orders of magnitude less than CO, in agreement with previous investigations. Analysis of CO emission spectra obtained over a variety of altitudes on Titan's nightside limb indicates that the stratospheric abundance of CO is 32 ± 15 ppm, and together with other recent determinations, suggests a vertical distribution of CO nearly constant at this value from the surface throughout the troposphere to at least the stratopause near 300 km altitude. The corresponding total atmospheric content of CO in Titan is $\sim 2.9 \pm 1.5 \times 10^{14}$ kg. Given the long lifetime of CO in the oxygen-poor Titan atmosphere (~ 0.5–1.0 Gyr), we find a mean CO atmospheric production rate of $6 \pm 3 \times 10^5$ kg yr^{-1}. Given the lack of primordial heavy noble gases observed by Huygens [Niemann et al., 2005. The abundances of constituents of Titan's atmosphere from the GCMS on the Huygens probe. Nature, 438, 779–784], the primary source of atmospheric CO is likely surface emissions. The implied CO/CH_4 mixing ratio of near-surface material is $1.8 \pm 0.9 \times 10^{-4}$, based on an average methane surface emission rate over the past 0.5 Gyr of 1.3×10^{-13} gm cm^{-2} s^{-1} as required to balance hydrocarbon haze production via methane photolysis [Wilson and Atreya, 2004. Current state of modeling the photochemistry of Titan's mutually dependent atmosphere and ionosphere. J. Geophys. Res. 109, E06002 Doi:10.1029/2003JE002181]. This low CO/CH_4 ratio is much lower than expected for the sub-nebular formation region of Titan and supports the hypothesis [e.g., Atreya et al., 2005. Methane on Titan: photochemical-meteorological-hydrogeochemical cycle. Bull. Am. Astron. Soc. 37, 735] that the conversion of primordial CO and other carbon-bearing materials into CH_4-enriched clathrate-hydrates occurs within the deep interior of Titan via the release of hydrogen through the serpentinization process followed by Fischer–Tropsch catalysis. The time-averaged predicted emission rate of methane-rich surface materials is ~ 0.02 km^3 yr^{-1}, a value

---

*Corresponding author. Tel.: +1 818 354 0481; fax: +1 818 393 5148.

E-mail addresses: kbaines@aloha.jpl.nasa.gov (K.H. Baines), Pierre.Drossart@obspm.fr (P. Drossart), valverde@iaa.es (M.A. Lopez-Valverde), atreya@umich.edu (S.K. Atreya), sotin@chimie.univ-nantes.fr (C. Sotin), momary@mail1.jpl.nasa.gov (T.W. Momary), rhb@lpl.arizona.edu (R.H. Brown), bonnie.buratti@jpl.nasa.gov (B.J. Buratti), rclark@usgs.gov (R.N. Clark), nicholso@astro.cornell.edu (P.D. Nicholson).

significantly lower than the rate of silicate lava production for the Earth and Venus, but nonetheless indicative of significant active geological processes reshaping the surface of Titan.

1. Introduction

As revealed in spectral images acquired by the Visual Infrared Mapping Spectrometer (VIMS) onboard the Cassini orbiter (Baines et al., 2005), Titan glows at night (c.f., Fig. 1). Nighttime emissions near 4.5 μm extend several 100 km altitude above the surface (Fig. 2). Three emission features are discernable in the 4.1–4.8 μm spectral range (Fig. 3), corresponding to the spectral location of the P and R branches of the 1-0 vibrational band of CO near 4.65 μm and the strong CH_3D v_2 Q branch near 4.55 μm. The intrinsically strong 4.3-μm v_3 vibrational band of CO_2 is here much weaker than the CH_3D emission, indicating a CO_2 abundance several orders of magnitude less than either CH_3D or CO, qualitatively consistent with infrared spectral measurements obtained by Voyager IRIS (Coustenis et al., 1989, 1991; Samuelson et al., 1983) and Cassini CIRS (De Kok et al., 2005).

Beyond the spectral domain, the VIMS Titan spectral images also potentially reveal vertical information from the surface to over 350 km altitude, from which the mixing ratio and total content of CO in the atmosphere can be estimated. As noted previously (Lara et al., 1996; Wong et al., 2002; Lellouch et al., 2003; Wilson and Atreya, 2004), CO represents the major reservoir of oxygen within the atmosphere. Due primarily to photolysis and the resulting radical-based chemistry within the

hydrocarbon-rich upper atmosphere of Titan, all oxygen atoms are incorporated into CO, eventually. This occurs regardless of whether the parent volatiles are delivered externally by infalling comets or meteorites (e.g., H_2O, CO_2), or are released from the surface as, for example, cryovolcanic emissions. For external sources, the extant water vapor content (cf., Coustenis et al., 1998) can be used to constrain the production of CO. Thus, as has been performed by Lara et al. (1996) and Wong et al. (2002), an estimate of the surface flux of CO can be obtained from modeling the oxygen-based chemistry and comparing to the observed CO column abundance.

Theoretically, the vertical distribution of CO throughout the atmosphere should be uniform, given the long chemical lifetime of CO (~1 Gyr; Yung et al., 1984; Wong et al., 2002). However, evidence for enhancement of the CO mixing ratio in the upper levels of the atmosphere has come from (1) recent dayside near-IR observations from the ground (Lopez-Valverde et al., 2005) and (2) intercomparison of millimeter-wave measurements of the CO mixing ratio at different altitudes (e.g., Gurwell and Muhleman, 1995, 2000; Hidayat et al., 1997, 1998). Such a vertical gradient in the CO-mixing ratio could indicate a recently enhanced flux of oxygenated species, such as from a recent cometary impact, or an unspecified CO-destroying chemical pathway in the lower atmosphere, both of which greatly complicate assessments of CO outgassing from the interior.
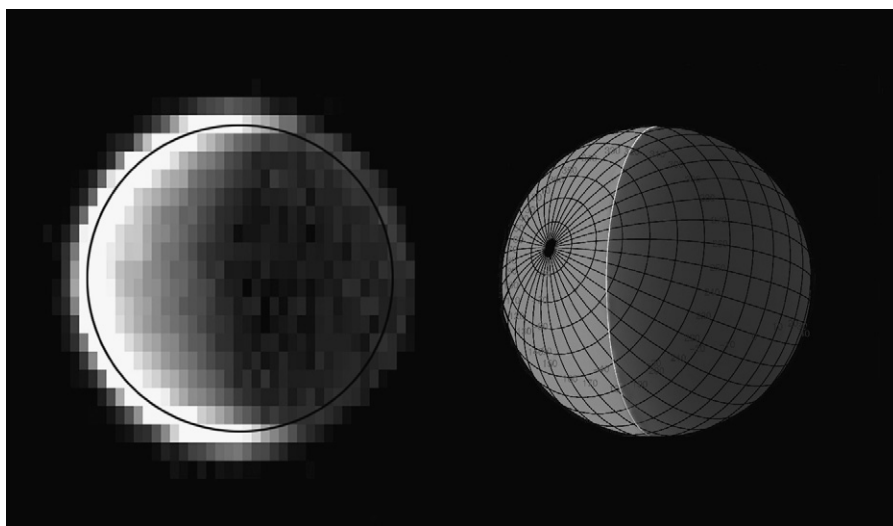

Fig. 1. Emissions revealed on the nightside of Titan (left) by Cassini/VIMS near 4.7 μm. As depicted in the observation geometry figure (right), Titan was spectrally imaged from over the southern hemisphere near 109° phase angle. The image shown is comprised of a spectral average of 12 VIMS band images from 4.6 to 4.8 um. The nightside limb (right side of disk) was oriented away from Saturn and its ring system, thereby ensuring extremely low levels of scattered sunlight from the Saturn system impinging on Titan's nightside. This observation, CM1467517212, was acquired on July 3, 2004 at a distance of 0.621 million km from Titan. The data were acquired in high-resolution mode (0.25 mrad IFOV in the lateral, left-right direction and 0.50 mrad IFOV in the vertical, up-down direction). Exposure time was 400 ms per pixel.
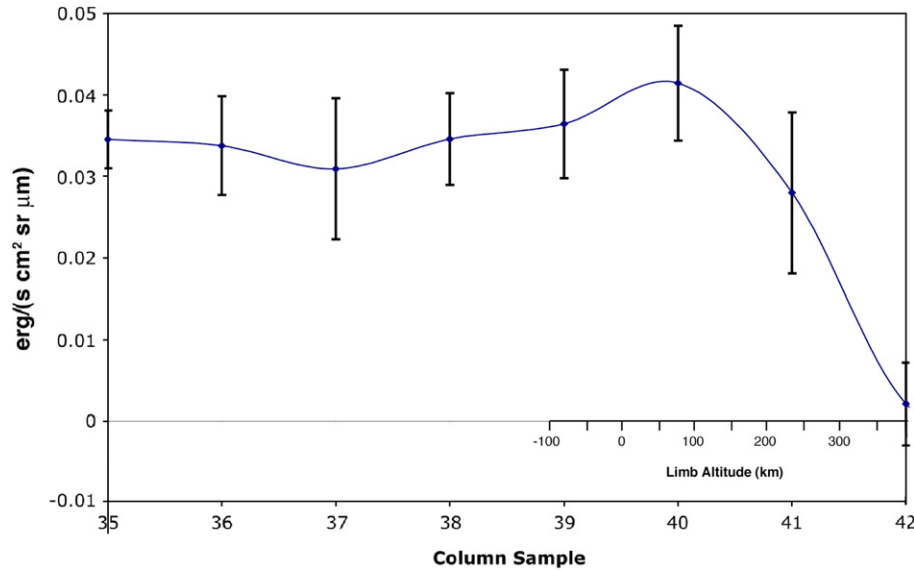
Fig. 2. Nighttime altitude profile of 4.6–4.8-μm integrated thermal emissions. A lateral limb profile was extracted, centered along the row of pixels oriented perpendicular to the Titan surface through the image cube shown in Fig. 1. For each altitude point on the profile, the five closest pixels in the cross-lateral (i.e., column) direction were averaged together to determine a mean spectrum per altitude point. The integrated thermal emission for each spectrum was then determined by averaging together all wavelengths in the relevant 4.6–4.8-μm spectrum. Error bars depict the standard deviation among the five points used for each average. The altitude relative to the limb is noted in the bottom scale.

On the other hand, intercomparison of ground-based data (e.g., Lellouch et al., 2003) with higher-altitude millimeter data (Hidayat et al., 1998), as well as the recent results of the CIRS instrument on Cassini (Flasar et al., 2005), indicates a nearly constant mixing ratio over altitude.

In the upper warm stratosphere, VIMS provides enhanced near-infrared estimates of CO abundance by observing nightside, rather than dayside, thermal emissions. Prior to the orbital reconnaissance by the Cassini spacecraft, near-infrared CO features on Titan were observed on the dayside—the only hemisphere visible from Earth. These observations provided conflicting results. Using near-IR reflection spectroscopy in the 1.6 μm spectral region, Lutz et al. (1983) first discovered CO in absorption. They determined a mixing ratio of 60 ppm, within a factor of three, using a simple reflecting layer analysis. Noll and Knacke, (1993) subsequently detected the 1-0 CO band in the 4.5–4.8 μm region with low-resolution ($R = 50$) spectrometry. Exploring this region with higher spectral resolution ($R = 1500$), Noll et al. (1996) derived a tropospheric mixing ratio of 10 ppm, significantly lower than the determinations by Lutz et al. (1983). Higher spectral resolution observations ($R{\sim}2000$) of the 1-0 and 2-1 CO bands by Lellouch et al. (2003) enabled increased accuracy, and suggested a mean tropospheric abundance of 32 ppm. However, analysis of these observations as well as the Lopez-Valverde et al. (2005) measurements proved difficult, as their interpretation was complicated by indefinite non-LTE effects prevalent on the dayside (cf. Lellouch et al., 2003, 2004; Lopez-Valverde et al., 2005). VIMS observations of the nightside are unaffected by this difficulty.

2. Observations and data reduction

VIMS observed Titan repeatedly during the first Cassini orbiter encounter with Saturn's largest satellite on July 3, 2004. Inbound on the close flyby, an especially favorable geometry for imaging nightside emissions on Titan occurred, wherein the nightside limb faced away from Saturn and its bright retinue of rings. Thus, the VIMS spectra are particularly noteworthy in that the only known source of 4–5-μm radiation producing the observed flux is thermal emission within the atmosphere. Here, we used the spectral image CM1467517212 (cf. Fig. 1), which was obtained in high-spatial-resolution mode (i.e., with an IFOV of 0.25×0.50 mrad). To obtain limb profiles at the highest possible spatial resolution, the high-spatial-resolution dimension was oriented in the direction perpendicular to the midnight limb (cf. Fig. 1). From a distance of 0.624 million km, the VIMS IFOV corresponded to 156 km in the high-spatial-resolution dimension. To achieve good signal-to-noise (S/N), a relatively long integration time of 400 ms per pixel was used.

Photometric and geometric calibrations were performed using standard VIMS calibration procedures (Brown et al., 2004; McCord et al., 2004). To improve the S/N of the spectrum for each of four altitudes, five adjacent pixels were averaged together along the low-spatial-resolution (column) dimension. In these averages, the central pixel of each five-pixel sample was located along the high-spatial-resolution-oriented row of pixels, which perpendicularly intercepted Titan's nightside limb. Taken as a set, these averaged spectra comprised the limb profile of spectra modeled in our analysis at four specific limb altitudes centered from 78 km inside the limb outward to 390 km
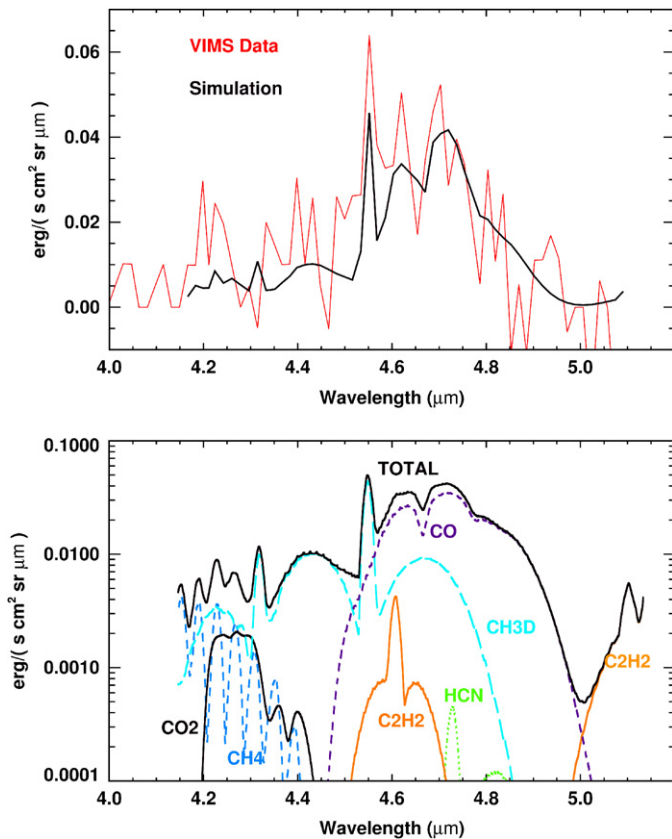
Fig. 3. The thermal emission spectrum at the limb. Top panel: observed VIMS spectrum (red) is compared against a synthetic spectrum (black), in linear scale. Bottom panel: Individual contributions to the net synthetic emission spectrum by CO (purple), CH_3D (aqua), CH_4 (blue), CO_2 (black), C_2H_2 (orange) and HCN (green) are shown, in log scale. Three prominent emissions are observed, the P and R branches of the 1-0 band of CO and the strong ν_2 fundamental of CH_3D near 4.5 μm. The weak CH_3D and CO_2 emissions modeled at 4.3 μm are below the measurement noise level, $0.01\,erg\,s^{-1}\,sr^{-1}\,cm^{-2}\,\mu m^{-1}$. The spectrum used here is for the pixel located immediately to the left of the limb shown in Fig. 2, spanning limb altitudes from −156 to 0 km altitude.

limb altitude at a limb-tangent latitude of 30° north latitude.

3. Spectral analysis

Simulations of the VIMS spectra were performed with a thoroughly validated line-by-line radiative transfer model (Dudhia, 2000), using spectral parameters from Hitran 2004 (Rothman et al., 2005). Spectral limb radiances emitted for an effective 900-km thick Titan atmosphere were calculated under nighttime conditions. Calculations were performed at four tangent altitudes, corresponding to the minimum altitude in the line-of-sight sampled at the midpoint of each pixel position in the VIMS vertical profile: 0, 78, 234 and 390 km altitude. A field of view of 156 km centered at these altitudes was used. We included in our analysis CO_2, CO, CH_4 (including CH_3D), C_2H_2, HCN and H_2O, with vertical mixing ratio profiles from the photochemical model of Lara et al. (1996). Following the

value recently measured at lower tropospheric altitudes by Lellouch et al. (2003) from disk averaged 5-μm ground-based observations, we initially adopted a constant CO volumetric mixing ratio (VMR) of 32 ppm. For CH_3D we used a constant VMR profile of 1.0×10^{-5}, consistent with that reported by Coustenis et al. (1989). The nominal thermal structure was taken from Yelle et al. (1997). Thermodynamic equilibrium (LTE) was assumed for all species. As shown for CO by Lopez-Valverde et al. (2005), departures from LTE for all the species considered under nighttime conditions are small at stratospheric altitudes. The calculations were performed between 1950 and $2400\,cm^{-1}$ (4.15–5.15 μm) with a spectral resolution of $0.001\,cm^{-1}$, degraded to the VIMS near-constant resolving power of ~275 over this spectral range by convolution with a triangular instrumental line shape of $8\,cm^{-1}$ width at half maximum.

In Fig. 3, the individual contributions from relevant species to the emerging radiance at a tangent altitude of 0 km are depicted, and the total outgoing radiance is compared to the VIMS data. The three strongest features are the emissions due to the P and R branches of the CO (1-0) band around 4.6 and 4.7 μm and that of the CH_3D ν_2 fundamental at 4.55 μm. The CH_3D $2\nu_6$ fundamental and CO_2 ν_3 vibrational band, both near 4.3 μm, give a negligible contribution, well below the noise level of $0.01\,erg\,s^{-1}\,cm^{-2}\,sr^{-1}\,\mu m^{-1}$. Methane gives a small contribution around 4.2 μm. H_2O, C_2H_2 and HCN are completely negligible. There is, however, a significant emission at 4.5 μm not reproduced by our simulation. Its variation with altitude is approximately similar to the other emission features, which indicates that it must be of thermal origin and due to a species not included in our simulation.

Synthetic emission spectra for each of the tangent altitudes are compared to the VIMS observations in Fig. 4. For the first three tangent altitudes, with the fields-of-view centered at the surface (0 km), 78 and 234 km, respectively, there is good general agreement between the simulation and the VIMS data for the major emissions. At 390 km altitude, the emissions are significantly weaker and noisier, with oscillations significantly larger than the simulated emission. Nevertheless, there is a distinct feature at the center of the CH_3D band, which stands clearly above the random noise oscillations and, if real, would indicate a much larger emission or abundance from CH_3D in the upper stratosphere of Titan. A 10-fold increase in the CH_3D mixing ratio, not supported observationally, still under-estimates the peak by 50% and strongly overestimates the emission at other wavelengths. The application of an alternative thermal structure with a fictitious profile 10 K warmer in the stratosphere, following Lopez-Valverde et al. (2005), also does not resolve this discrepancy. Further analysis is ongoing and is expected to be a subject of a subsequent paper.

In order to determine the range of altitudes that contribute significantly to the limb emission observed in
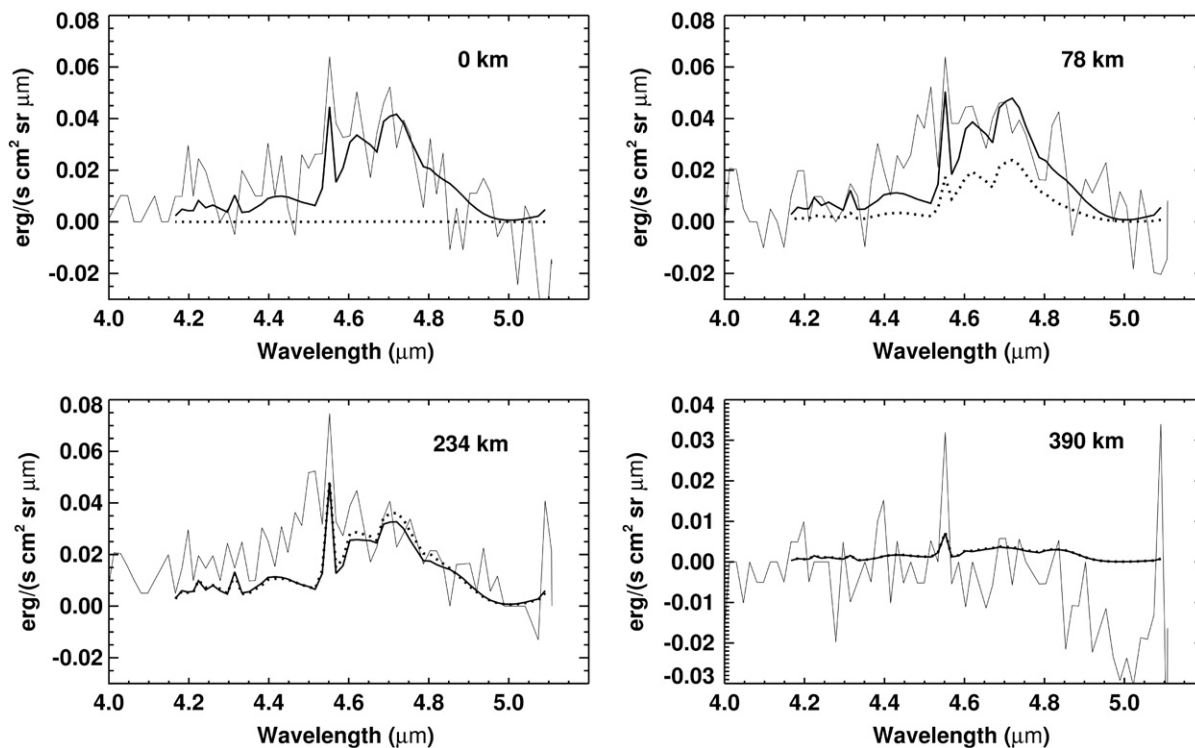
Fig. 4. Comparison of simulated spectra (solid thick lines) with the VIMS observations at four tangent altitudes—0, 78, 234 and 390 km altitude—assuming (1) a CO mixing ratio of 32 ppm and (2) the nominal thermal structure of Yelle et al. (1997). Good general agreements between the simulations and observed VIMS CO spectra near 4.65 μm are obtained, given the measurement noise of ~0.01 erg s^{-1} sr^{-1} cm^{-2} μm^{-1}. Also shown (dotted lines) are spectra calculated by ignoring atmosphere emissions above the maximum tangent altitude sampled within each FOV. Only the relatively high-altitude observations centered near 78 and 234 km tangent altitude show meaningful emissions in the dotted spectra, indicating that emissions at Titan's limb originate between approximately 100 and 310 km altitude. In this figure, the labeled tangent altitudes denote the minimum altitudes sampled at the FOV centers. For the pixel located immediately to the left of the limb shown in Fig. 2, the tangent altitude is defined as 0 km, since the minimum altitude sampled throughout the pixel is at the surface.

each 5-pixel limb field-of-view (FOV), we now assess the contribution to the observed emissions within the tangent altitude range of each FOV. For this, we neglect the shell of the atmosphere residing above the maximum altitude of the FOV for each limb data point. Thus, we cut the atmosphere above the 156, 312 and 468 km altitude levels respectively, for the three highest limb-altitude points mentioned above. In this manner we extract the contribution to the emerging radiance, which is solely coming from the region at the tangent point, depicted as the dotted lines in Fig. 4. The difference with the total emission (itself shown as the solid lines) then illustrates the contribution from the atmospheric shell of layers above the maximum tangent altitudes. For the lowest altitude point, sampling the surface throughout the FOV, we conservatively used 78 km as the maximum FOV tangent altitude in our calculations, despite the fact that the maximum tangent altitude sampled by this point was 0 km throughout the FOV. Nevertheless, the modeled spectra show that virtually all of the emission actually comes from higher up in the atmosphere, above the 78-km level. Thus, this analysis demonstrates the troposphere does not contribute to the observed emission. Thus, VIMS spectra cannot measure tropospheric CO emissions to determine the CO abundance in this region of the atmosphere. In the case of

the observation centered at 78 km, the contribution from the overlying shell of atmosphere above 156 km is at least as important as the contribution from the tangent altitudes sampled within the FOV of the pixel. In contrast, the observation centered at 234 km receives virtually all of its emission from the range of tangent altitudes within the FOV. It is interesting to note that, at this tangent altitude, the solid line is less than the dotted line, indicating that the overlying layers actually represent net absorption. In the highest tangent altitude, centered near 390 km, the overlying atmospheric region is also irrelevant. Thus, this analysis indicates that significant contributions to the observed emissions in all of the pixels sampled across the limb of Titan come from approximately the 100–~310 km altitude range encompassing the warmest portion of the stratosphere.

In all these simulations we used the nominal temperature profile mentioned above. The actual temperature is, however, not precisely known at our observed latitude of 30 N, and it may be subject to significant latitudinal variability (Coustenis and Bézard, 1995; Flasar et al., 2005). We thus used the prominent CH$_3$D emission to constrain the actual thermal profile at 30 N, as shown in Fig. 5. In the upper panel we compare the nominal profile (green curve) to a significantly warmer profile determined
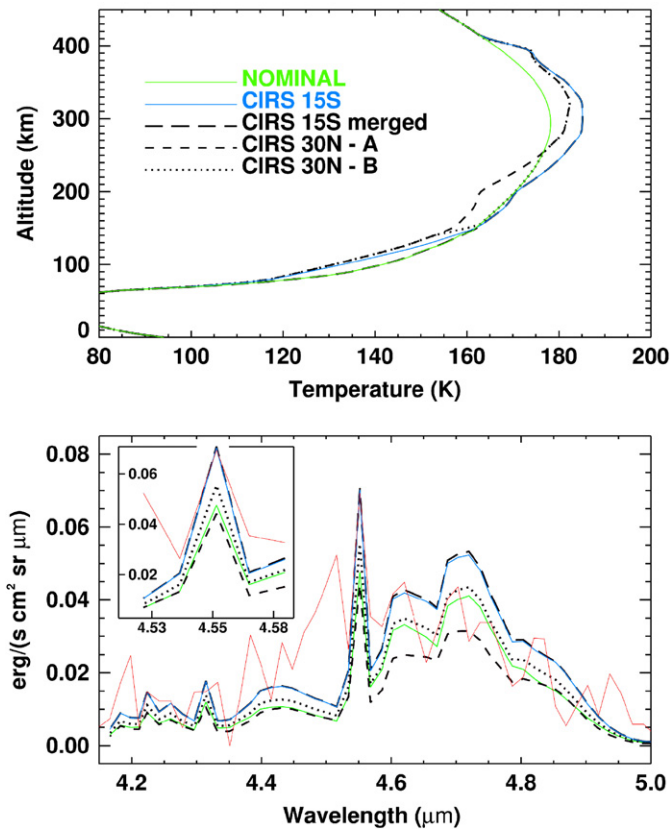
Fig. 5. Effect of the stratospheric thermal structure on the emerging spectra. A variety of thermal structures (top panel) were tested. Simulations for each of these five different thermal profiles are shown in the bottom panel and inset, for a FOV 312-km wide centered at a tangent altitude of 156 km. An appropriate VIMS stratospheric averaged spectrum (from the two spectra centered at 78 and 234 km in Fig. 4) is shown in red for comparison. The best fit to the prominent CH_3D emission feature at 4.55 μm is obtained for the CIRS temperature profile at 15 S, as shown in the inset.

for 15 S latitude from CIRS data (Flasar et al., 2005; blue curve). We modified this 15 S profile according to the latitudinal variation of temperature in the lower stratosphere, below about 250 km, as presented in Fig. 1 of Flasar et al. (2005), which indicates that the kinetic temperature of each of our FOVs may be about 2, 5, 8 and 5 K colder, respectively, at 30 N than at 15 S.

As depicted in Fig. 5, we evaluated five candidate temperature profiles. Besides the nominal profile (green) and the warmer CIRS 15 S profile (blue in Fig. 5), we evaluated a merged profile following the warm 15 S profile above 200 km altitude and the nominal profile below that level (long-dashed in Fig. 5). An additional profile, "CIRS 30 N-A" (short-dashes in Fig. 5), tends to the CIRS 15 S profile above 250 km, following the latitudinal variability noted by CIRS. A final profile, called "CIRS 30 N-B" (dotted line in Fig. 5), combines this CIRS 30 N-A profile with the nominal temperature profile (green) below 200 km. The spectra computed for all of these thermal structures are compared to a VIMS spectrum in the lower panel

of Fig. 5. Here, the VIMS spectrum corresponds to an average of the 78 and 234 km tangent observations, and thus has an effective FOV spanning the surface to about 312 km altitude.

As shown most clearly in the inset in Fig. 5, the best fit to the CH_3D peak emission is obtained for profiles incorporating the warm CIRS 15 S temperature profile. Colder thermal profiles above the 200-km level give worse fits to the VIMS data. In particular the 30 N-A case yields a very poor match to the CH_3D emission. Within the uncertainty in the CH_3D vmr, the CIRS 15 S profile would therefore be our best choice for the thermal structure. Our nominal temperature and the 30 N-B case give better radiances and spectral fits than the 30 M-A case, underestimating the CH_3D peak by about $0.01 \, erg \, s^{-1} \, cm^{-2} \, sr^{-1} \, \mu m^{-1}$, which corresponds to the measurement noise. Thus, we consider the difference between the CIRS 15 S and the CIRS 30 N-B profiles as the uncertainty in the temperature structure at 30 N latitude for our analysis.

In Fig. 6 we display simulated spectra for a variety of CO mixing ratios, using the CIRS 15 S temperature profile. Specifically, we used 10, 45 and 60 ppm, as well as 32 ppm. The largest value of 60 ppm was recently determined at stratospheric altitudes from CO non-LTE emissions in disk-averaged ground observations in the 5-μm windows (Lopez-Valverde et al., 2005). These authors found a consistent fit to both their tropospheric absorption measurement (Lellouch et al., 2003) and to the stratospheric emission data using a factor-of-two vertical gradient in the CO mixing ratio, although the stratospheric value could be significantly affected by indefinite non-local LTE processes. In contrast, here, we find that the VIMS spectra pertaining to the warm stratosphere are consistent with a vertically constant mixing ratio of 32 ppm. In particular, Fig. 6 shows that a CO VMR of 60 ppm overestimates the emission in the CO fundamental P branch, while the lowest value of 10 ppm clearly underestimates the R branch. The value of 32 ppm does also overestimate the P branch, but within the measurement noise bracket. Considering the noise and the thermal flux uncertainties, both of the order of $0.01 \, erg \, s^{-1} \, sr^{-1} \, cm^{-2} \, \mu m^{-1}$, an uncertainty of the order of 15 ppm around 32 ppm is consistent with this VIMS spectrum.

This derivation was based on the temperature fit of the CH_3D peak emission at 4.55 μm. A sensitivity study indicates that a factor of three increase in the CH_3D abundance would produce an increase in the peak emission on the order of the radiance noise, and about half that amount in the CO P and R branches. With such an enhanced CH_3D abundance the 30 N-B temperature profile might be a better choice than the CIRS 15 S. This illustrates that the uncertainty in the temperature structure and in the CH_3D abundance are linked in this analysis. With such a combination of temperature and CH_3D as the optimum choice, the derived CO VMR would be a bit larger than 32 ppm and still smaller than 45 ppm; in other words, within the bracket suggested above.
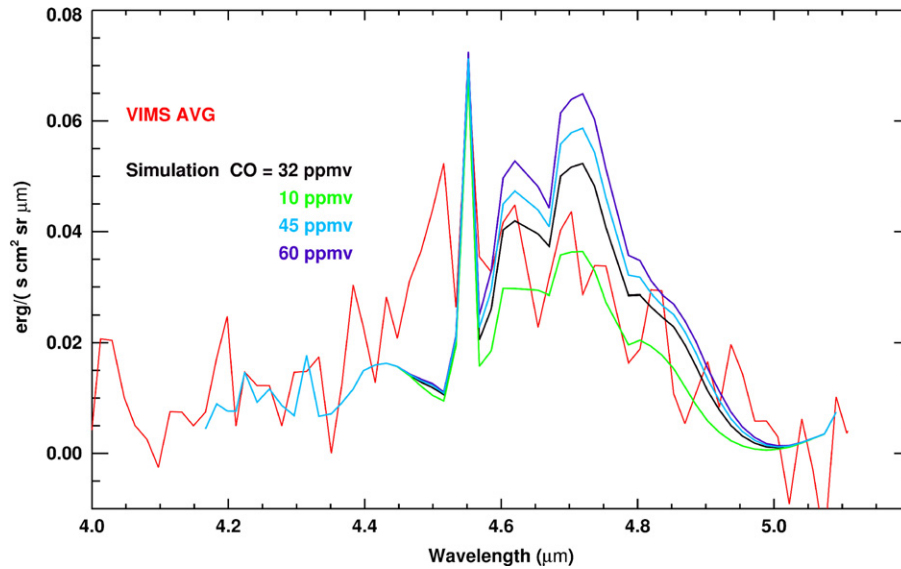
Fig. 6. CO models compared to the stratospheric averaged VIMS spectrum spanning tangent altitudes from 0 to 312 km. The VIMS spectrum is the average of the two spectra centered at 78 and 234 km in Fig. 4. Spectra are shown assuming vertically constant CO abundances of 10, 32, 45 and 60 ppm. A CO mixing ratio of 32 ± 15 ppm is indicated as the viable range of solutions.

We note that our value pertaining to the $\sim$100–310 km altitude region also is compatible with the CIRS/Cassini (Flasar et al., 2005) measurement of 45 ± 15 ppm for the 130–230 km altitude region. When these stratospheric results are combined with the ground-based determinations (Lellouch et al., 2003), the result is that CO is uniformly mixed in the Titan atmosphere, to within $\sim$50%, from the troposphere to the upper stratosphere.

4. Geological implications

In the upper atmosphere of Titan, solar ultraviolet photolysis of methane leads to the creation of higher-order hydrocarbon gases and hazes and thence to the precipitation of organic compounds onto the surface (Strobel, 1974; Lunine et al., 1983; Flasar, 1983; Yung et al., 1984; Wilson and Atreya, 2004). To replenish this loss of atmospheric carbon, a source of methane must exist at or underneath the surface of Titan. Thus, subsurface processes with surface expressions of gaseous and/or liquid methane are indicated, with perhaps relatively rapid release in the form of cryovolcanic emissions. Indeed, such a geologic feature may have been observed in the first high-spatial-resolution (km-scale) surface image obtained by both the VIMS and the Radar experiments onboard the Cassini spacecraft (Sotin et al., 2005; Elachi et al. 2005). If the atmosphere existed in its present form over the age of the solar system, it is predicted that organic materials, including liquids, sufficient to cover the entire surface to a depth of several 100 m would have precipitated out of the skies of Titan. Recent observations by the Huygens probe and Cassini spacecraft do not show large regions of liquid on the surface, although some liquid deposits are not ruled out (Elachi et al., 2005), and evidence of surface flows has been imaged by the Huygens probe (Tomasko et al., 2005). It is apparent then that understanding the nature of the surface–atmosphere interactions is critical to understanding the evolution of the interior, surface, and atmosphere of Titan.

A vertically-uniform CO distribution of 32 ppm amounts to a total atmospheric CO content of 2.9×10^{14} kg, assuming (1) a surface pressure of 1498 mb, (2) a methane mole fraction of 5% in the lower troposphere as observed by the GCMS (Niemann et al., 2005) and DISR (Tomasko et al., 2005) experiments onboard the Huygens probe/lander, (3) a Titan surface gravity, g, of 1.355 m s^{-2}, and (4) a surface radius of 2575 km. A rough estimate of the CO production rate required to maintain a steady-state CO mixing ratio of 32 ppm in the atmosphere can be obtained by dividing the CO mass by its lifetime on Titan, which is on the order of 10^9 years (Wong et al., 2002). Thus the photochemical destruction rate of CO is on the order of $\sim$3 $\times$ 10^5 kg yr^{-1}, which under equilibrium conditions then represents the re-supply rate from the surface and/or interior, assuming a negligible contribution from external sources such as meteorites and comets.

A more accurate determination of the strength of the internal source of CO takes into consideration the full chemical process of production and loss of CO on Titan, accounting in particular for chemistry involving water delivered by external sources. In the past, such chemistry has been shown to account for a large fraction of the observed CO (Yung et al., 1984, Lara et al., 1996). However, contrary to previous models (e.g. Yung et al., 1984), Wong et al. (2002) conclude that the reaction between CH$_3$ (produced in the photolysis of CH$_4$) and OH (produced in the photolysis of externally delivered H$_2$O), is not the major pathway for the production of CO on Titan. In fact, even after including all catalytic reactions between CH$_4$ and H$_2$O for producing CO, it is found that for CO to

be in equilibrium, with no external or internal source of CO, the CO-mixing ratio would be 1.8 ppm or roughly 5% of the observed value. Wong et al. (2002) require a source flux of $1.1 \times 10^6 \, \text{cm}^{-2} \, \text{s}^{-1}$ CO molecules in order to explain their assumed 52 ppm of CO. This value is scaled to $6.8 \times 10^5 \, \text{cm}^{-2} \, \text{s}^{-1}$ for our best fit measured 32 ppm of CO. This then amounts to a source flux of $7.8 \times 10^5 \, \text{kg yr}^{-1}$, a little over twice the amount of our simple lifetime-based estimate above. Lara et al. (1996) assumed twice the flux of H_2O molecules from meteorites, comets, etc. compared to Wong et al. (2002) (3.0×10^6 vs. $1.5 \times 10^6 \, \text{cm}^{-2} \, \text{s}^{-1}$), resulting in a smaller internal CO source flux of $5.1 \times 10^5 \, \text{cm}^{-2} \, \text{s}^{-1}$, or approximately $5.9 \times 10^5 \, \text{kg yr}^{-1}$, again scaled for our current best-fit CO abundance of 32 ppm.

According to an alternate scenario proposed by Lara et al. (1996), an external CO flux of $1.6 \times 10^6 \, \text{cm}^{-2} \, \text{s}^{-1}$ delivered, for example, by meteorites or comets, can completely explain the observed CO abundance on Titan. However, the recent lack of detection of primordial noble gases in Titan's atmosphere by the Huygens GCMS, except for very tiny traces of ^{36}Ar (Niemann et al., 2005), indicates that comets and other external sources have not been significant transporters of material to Titan over the aeons. Thus, the bulk of the observed CO must come from inside Titan.

Another potential indicator of internally released CO comes from the low stratospheric abundance of CO_2. The orders-of-magnitude greater amount of CO compared to the CO_2 abundance, both as observed in our spectra as well as in CIRS measurements of the unsaturated stratosphere (De Kok et al., 2005), is contrary to the value of 1.3 for CO/CO_2 estimated for cometary nuclei (Boice and Huebner, 1997). The CO_2-mixing ratio in the upper atmosphere measured by CIRS is several orders of magnitude less than the local saturation abundance (De Kok, private communication), and thus perhaps indicates a steady-state situation where comet-supplied CO is a small fraction of the observed CO column abundance. However, this measured stratospheric CO_2-mixing ratio is still several orders of magnitude greater than the saturated-mixing ratio at the tropopausal cold-trap, and is thus not inconsistent with a large steady-state comet flux scenario allowing for vertical transport and rainout of CO_2 at the tropopause. Consequently, the extremely low-stratospheric CO_2 abundance compared to CO is not in itself direct evidence of CO surface emission, but is consistent with this hypothesis.

The loss of CO in the atmosphere of Titan is mainly by its reaction with OH, with some assistance by photolysis occurring near 0.27 μm. With a photochemical lifetime on the order of a billion years, CO is expected to be uniformly mixed, as we find to be the case in the VIMS data analyzed here combined with previous measurements at lower altitudes (e.g., Lellouch et al., 2003). From above considerations, we conclude that an internal source of approximately $6 \pm 3 \times 10^5 \, \text{kg yr}^{-1}$ of CO is required to maintain CO in its current VMR of 32 ± 15 ppm.

The source of internal CO could be cryovolcanic activity. As noted earlier, both the VIMS and Radar experiments onboard the Cassini spacecraft may have actually captured such geologic features in their first km-scale images (Sotin et al., 2005; Elachi et al., 2005). Surface emission of methane, including cryovolcanic activity, has been invoked to balance the loss of atmospheric methane via photochemistry and subsequent rainout of hydrocarbon-based condensates and hazes (e.g. Atreya et al., 2005).

Recent models of Titan's evolution (Tobie et al., 2006) suggest that Titan has experienced three major episodes of methane release into the atmosphere. According to these models, the current geologic epoch started about 500 Myr ago when the thickness of the outer ice layer became large enough for subsolidus convection to begin and cool the satellite. During this episode, convective upwellings are bringing clathrate-hydrates close to the surface. The clathrates destabilize during this adiabatic decompression and release the encaged volatile species (CO and CH_4) into the atmosphere.

The amount of surface CO released during the present 0.5 Gyr-long epoch is $3.0 \pm 1.5 \times 10^{14} \, \text{kg}$. During this same period, the amount of methane released can be estimated from the current rate of methane loss in the photochemical production of heavy hydrocarbon-based condensates and hazes as determined by Wilson and Atreya (2004). The methane loss to precipitating aerosols of $4.8 \times 10^9 \, \text{molecules cm}^{-2} \, \text{s}^{-1}$ corresponds to a methane surface release rate of $1.3 \times 10^{-16} \, \text{kg cm}^{-2} \, \text{s}^{-1}$, assuming the methane content of the atmosphere remains constant during the epoch. Over the 0.5 Gyr of the current epoch, the Wilson and Atreya (2004) hydrocarbon aerosol production rate amounts to $1.7 \times 10^{18} \, \text{kg}$ of methane released into the Titan atmosphere to maintain equilibrium. Thus, comparing the total global amounts of CO and CH_4 produced during the current epoch, we find a volumetric CO/CH_4 ratio of $1.8 \pm 0.9 \times 10^{-4}$.

We note that this ratio is in agreement with recent measurements of hydrothermal systems on Earth (Fiebig et al., 2004) where the reduction of CO into CH_4 is obtained by the Fischer–Tropsch catalysis process involving hydrogen rather than thermogenic processes involving organic matter. This agreement suggests that Titan's methane also may have been produced by the Fischer–Tropsch catalytic process (e.g., Prinn and Fegley, 1989), either (1) in Saturn's sub-nebula as proposed by Sekine et al. (2005) and then trapped and transported to Titan in clathrates (e.g., Hersant et al., 2004) or (2) at depth within Titan, in clathrates formed via the serpentinization process as the source of reactive hydrogen created at the silicate/water interface, as proposed by Atreya et al. (2005). However, the low efficiency of the Fischer–Tropsch process argues against the thorough conversion of CO to CH_4 in the sub-nebula to obtain the low CO/CH_4 abundance of $\sim 1.8 \times 10^{-4}$ reported here. Thus, our analysis favors the formation of methane at depth in Titan via the combined processes of serpentinization and Fischer–Tropsch catalysis.

Assuming a volumetric ratio of 6:1 for H_2O:volatile in the clathrate materials, we find an annual amount of $0.02 \, km^3 \, yr^{-1}$ for material upwelled and exposed at the surface, corresponding to a global mean resurfacing rate of 24 cm per million years. However, this resurfacing is spread non-uniformly over the planet; instead, it is located above upwellings forming cryovolcanic features similar to the feature imaged by VIMS (Sotin et al., 2005). Although these cryovolcanic materials are not the same as involved in terrestrial volcanism, it is interesting to make the comparison since convection is the process involved for each of these solar system bodies. For the Earth and Venus, the annual rate of volcanism is 3 and $\sim 1 \, km^3 \, yr^{-1}$, respectively (Fegley and Prinn, 1989; Basilevsky and Head, 2002). If one scales these planets to Titan's surface area, one finds 0.6 and $\sim 0.2 \, km^3 \, yr^{-1}$, respectively. Titan's volcanism seems to provide significantly less eruptive material than on the two volcanically active terrestrial planets. The significantly larger value for the Earth is likely related to the existence of plate tectonics and the very large emission of lavas at mid-ocean ridges. The lesser amount of volcanic flows for Titan seems to suggest that tectonics plays a minor role, at best, there. This view is also supported by the images of Titan's surface obtained thus far by ISS, VIMS, and RADAR, which suggest that volcanism is localized, related only to the effects of 'hot plumes' above convective upwellings, similar to Venus. Nevertheless, one must keep in mind that the flow materials are very different and their domains of destabilization, and therefore the amount of volcanic flows erupting from each of these diverse planetary objects, cannot be compared easily.

5. Conclusion

In this paper, we have presented a quantitative assessment of the CO content in Titan's atmosphere, based on limb spectra acquired over a variety of tangent altitudes on Titan's nightside limb. We find the best-fit CO value is 32 ppm, with an uncertainty of ± 15 ppm. We have used this assessment to determine constraints on outgassing from Titan's surface. We find that the CO/CH_4 mixing ratio is $1.8 \pm 0.9 \times 10^{-4}$ if the amount of CH_4 is determined by its photolytic destruction and subsequent rainout of the associated complex hydrocarbons. Such a value is an agreement with the transformation of CO into CH_4 in the depths of Titan during the past ~ 0.5 Gyr by reactions involving (1) the release of hydrogen from water through the serpentinization process and (2) Fischer–Tropsch catalysis.

Our analysis of VIMS spectra, valid for the lower stratosphere, together with other recent determinations of CO in the upper stratosphere and in the troposphere (Lellouch et al., 2003; Lopez-Valverde et al., 2005; Flasar et al., 2005) indicates that CO is uniformly mixed, to an accuracy of about 50% throughout the atmosphere from the surface to above 300 km altitude. The CO profile is thus inconsistent with a recent episode of cometary impacts and is consistent with known chemical pathways.

We are currently planning future observations with longer exposure times and placed closer to the planet, so as to obtain the CO-mixing ratio with improved fidelity and at higher vertical resolution. In the upper stratosphere, these new observations should provide a valuable comparison of gas abundances as derived by CIRS and VIMS.

In conclusion we propose that delivery of CO into Titan's atmosphere from the interior by geologic processes involving outgassing is a plausible mechanism for maintaining a steady level of several tens of parts per million of CO on Titan. In particular, we find that the relatively low abundance of CO relative to CH_4 observed by Cassini/VIMS and others on Titan is consistent with the ideas that (1) methane within Titan's interior is largely formed by the conversion of CO and other oxygen-bearing carbon materials via the release of hydrogen through the serpentinization process followed by Fischer–Tropsch catalysis, and (2) this methane and other volatiles (such as the unprocessed CO at depth) are then delivered to the atmosphere via the convective upwelling of material and subsequent emission at the surface.

References

Atreya, S.K., Niemann, H.B., Owen, T.C., Adams, E.Y., Demick, J.E., 2005. Methane on Titan: photochemical-meteorological-hydrogeochemical cycle. Bull. Am. Astron. Soc. 37, 735.

Baines, K.H., Brown, R.H., Cruikshank, D.P., Clark, R.N., Nelson, R.M., Matson, D.L., Buratti, B., Carusi, A., Corodini, A., Bibring, J.P., Sotin, C., Jaumann, R., Formisano, V., Combes, M., Drossart, P., Langevin, Y., Sicardy, B., 2005. The atmospheres of Saturn and

Titan in the near-infrared: first results of Cassini/VIMS. Earth, Moon Planets 96, 119–147.

Basilevsky, A., Head, J.W., 2002. Venus: timing and rates of geologic activity. Geology 30, 1015–1018.

Boice, D.C., Huebner, W.F., 1997. Comet: structure and composition. In: Sirley, J.H., Fairbridge, R.W. (Eds.), Encyclopedia of Planetary Sciences. Chapman & Hall, London, pp. 145–153.

Brown, R.A., Baines, K.H., Bellucci, G., Bibring, J.-P., Buratti, B.J., Capacionni, F., Cerroni, P., Clark, R.N., Coradini, A., Cruikshank, D.P., Drossart, P., Formisano, V., Jaumann, R., Langevin, Y., Matson, D.L., McCord, T.B., Mennella, V., Miller, E., Nelson, R.M., Nicholson, P.D., Sicardy, B., Sotin, C., 2004. The Cassini Visual and Infrared Mapping Spectrometer investigation. Space Sci. Rev. 115, 1–4, 111–168.

Coustenis, A., Bézard, B., 1995. Titan's atmosphere from Voyager infrared observations. IV. Latitudinal variations of temperature and composition. Icarus 115, 126–140.

Coustenis, A., Bezard, B., Gautier, D., 1989. Titan's atmosphere from voyager infrared observations. II. The CH_3D abundance and D/H ratio from the 900–1200 cm^{-1} spectral region. Icarus 82, 67–80, (54–76).

Coustenis, A., Bezard, B., Gautier, D., Marten, A., Samuelson, R., 1991. Titan's atmosphere from voyager infrared observations. III. Vertical distributions of hydrocarbons and nitriles near Titan's north pole. Icarus 89, 152–167.

Coustenis, A., Salama, A., Lellouch, W., Encrenaz, T., Bjoraker, G., Samuelson, R.E., de Graauw, T., Feuchtgruber, H., Kessler, M.F., 1998. Evidence for water vapor in Titan's atmosphere from ISO/SWS data,. Astron. Astrophys. 136, L85–L90.

De Kok, R., Irwin, P.G.J., Teanby, N.A., Fletcher, L., Calcutt, S.B., Howett, C., Taylor, F.W., Bowles, N.E., and the Cassini/CIRS Team, 2005. Titan's oxygen compound distributions and condensate characteristics from Cassini/CIRS observations. Bull. Am. Astron. Soc. 37, 718.

Dudhia, A., 2000. Michelson Interferometer for Passive Atmospheric Sounding (MIPAS) Reference Forward Model (RFM). Software User's Manual. Oxford University Press, Oxford, UK.

Elachi, C., Wall, S., Allison, M., Anderson, Y., Boehmer, R., Callahan, P., Encrenaz, P., Flamini, E., Franceschetti, G., Gim, Y., Hamilton, G., Hensley, S., Janssen, M., Johnson, W., Kelleher, K., Kirk, R., Lopes, R., Lorenz, R., Lunine, J., Muhleman, D., Ostro, S., Paganelli, F., Picardi, G., Posa, F., Roth, L., Seu, R., Shaffer, S., Soderblom, L., Stiles, B., Stofan, E., Vetrella, S., West, R., Wood, C., Wye, L., Zebker, H., 2005. Cassini Radar views the surface of Titan. Science 308, 970–974.

Fegley Jr., B., Prinn, R.G., 1989. Estimation of the rate of volcanism on Venus from reaction rate measurements. Nature 337, 55–58.

Fiebig, J., Chiodini, G., Caliro, S., Rizzo, A., Spangenberg, J., Hunziker, J., 2004. Chemical and isotopic equilibrium between CO_2 and CH_4 in fumarolic gas discharges: generation of CH_4 in arc-magmatic-hydrothermal systems. Geochim. Cosmochim. Acta 68, 2321–2334.

Flasar, F.M., 1983. Oceans on Titan? Science 221, 55–57.

Flasar, F.M., Achterberg, R.K., Conrath, B.J., Gierasch, P.J., Kunde, V.G., Nixon, C.A., Bjoraker, G.L., Jennings, D.E., Romani, R.N., Simon-Miller, A.A., Bézard, B., Coustenis, A., Irwin, P.G.J., Teanby, N.A., Brasunas, J., Pearl, J.C., Segura, M.E., Carlson, R.C., Mamoutkine, A., Schinder, P.J., Barucci, A., Courtin, R., Fouchet, T., Gautier, D., Lellouch, E., Marten, A., Prangé, R., Vinatier, S., Strobel, D.F., Calcutt, S.B., Read, P.L., Taylor, F.W., Bowles, N., Samuelson, R.E., Orton, G.S., Spilker, L., Owen, T.C., Spencer, J.R., Showalter, M.R., Ferrari, C., Abbas, M.M., Raulin, F., Edgington, S., Ade, P., Wishnow, E.H., 2005. Titan's atmospheric temperatures, winds, and composition. Science 308, 975–978.

Gurwell, M.A., Muhleman, D.O., 1995. CO on Titan: evidence for a well-mixed profile. Icarus 117, 375–382.

Gurwell, M.A., Muhleman, D.O., 2000. CO on Titan: more evidence for a well-mixed vertical profile. Icarus 145, 653–656.

Hersant, F., Gautier, D., Lunine, J.I., 2004. Enrichment in volatiles in the giant planets of the Solar System. Planet. Space Sci. 52, 623–641.

Hidayat, T., Marten, A., Bezard, B., Gautier, D., Owen, T., Mathews, H.E., Paubert, G., 1997. Millimeter and submillimeter heterodyne observations of Titan: retrieval of the vertical profile of HCN and the $^{12}C/^{13}C$ ratio. Icarus 126, 170–182.

Hidayat, T., Marten, A., Bezard, B., Gautier, D., Owen, T., Matthews, G.H.E., Paubert, G., 1998. Millimeter and submillimeter heterodyne observations of Titan: the vertical profile of carbon monoxide in its stratosphere. Icarus 133, 109–133.

Lara, L.M., Lellouch, E., Lopez-Moreno, J.J., Rodrigo, R., 1996. Vertical distribution of Titan's atmospheric neutral constituents. J. Geophys. Res. 101, 23261–23383 (erratum: 1998,103, 25775).

Lellouch, E., Coustenis, A., Sebag, B., Cuby, J.-G., Lopez-Valverde, M., Schmitt, B., Fouchet, T., Crovisier, J., 2003. Titan's 5-µm window: observations with the very large telescope. Icarus 162, 125–142.

Lellouch, E., Schmitt, B., Coustenis, A., Cuby, J.-G., 2004. Titan's 5-micron lightcurve. Icarus 168, 209–214.

Lopez-Valverde, M.A., Lellouch, E., Coustenis, A., 2005. Carbon monoxide fluorescence from Titan's atmosphere. Icarus 175, 503–521.

Lunine, J.I., Stevenson, D.J., Yung, Y.L., 1983. Ethane ocean on Titan. Science 222, 1229–1230.

Lutz, B.L., de Bergh, C., Owen, T., 1983. Titan: discovery of carbon monoxide in its atmosphere. Science 220, 1374–1375.

McCord, T.B., and the VIMS Team, 2004. Cassini VIMS global observations of the galilean satellites including the VIMS calibration procedure. Icarus 172, 104–126.

Niemann, H.B., Atreya, S.K., Bauer, S.J., Carignan, G.R., Demick, J.E., Frost, R.L., Gautier, D., Haberman, J.A., Harpold, D.N., Hunten, D.M., Israel, G., Lunine, J.I., Ksprzak, W.T., Owen, T.C., Paulkovich, M., Raulin, F., Raaen, E., Way, S.H., 2005. The abundances of constituents of Titan's atmosphere from the GCMS on the Huygens probe. Nature, 438, 779–784.

Noll, K.S., Knacke, R.F., 1993. Titan: 1–5 µm photometry and spectro-photometry and a search for variability. Icarus 101, 272–281.

Noll, K.S., Geballe, T.R., Knacke, R.F., Pendleton, Y.J., 1996. Titan's 5 µm spectral window: carbon monoxide and the albedo of the surface. Icarus 124, 625–631.

Prinn, R.G., Fegley Jr., B., 1989. Solar nebula chemistry: origin of planetary, satellite, and cometary volatiles. In: Atreya, S.K., Pollack, J.B., Matthews, M.S. (Eds.), Origin and Evolution of Planetary and Satellite Atmospheres. University of Arizona Press, Tucson.

Rothman, L.S., et al., 2005. The HITRAN 2004 molecular spectroscopic database. J. Quant. Spectrosc. Radiat. Transfer 96, 2005.

Samuelson, R.E., Maguire, W.C., Hanel, R.A., Kunde, V.G., Jennings, D.E., Yung, Y.L., Aitkin, A.C., 1983. CO_2 on Titan. J. Geophys. Res. 88, 8709–8715.

Sekine, Y., Sugita, S., Shido, T., Yamamoto, T., Iwasawa, Y., Kadono, T., Matsui, T., 2005. The role of the Fischer–Tropsch catalysis in the origin of methane-rich Titan. Icarus 178, 154–164.

Sotin, C., Jaumann, R., Buratti, B.J., Brown, R.H., Clark, R.N., Soderblom, L.A., Baines, K.H., Belluci, G., Bibring, J.-P., Capaccioni, F., Cerroni, P., Combes, M., Coradini, A., Cruikshank, D.P., Drossart, P., Formisano, V., Langevin, Y., Matson, D.L., McCord, T.B., Nelson, R.M., Nicholson, P.D., Sicardy, B., LeMouelie, S., Rodriguez, S., Stephan, K., Scholz, C.K., 2005. Release of volatiles from a possible cryovolcano from near-infrared imaging of Titan. Nature 435, 786–789.

Strobel, D.F., 1974. The photochemistry of hydrocarbons in the atmosphere of Titan. Icarus 21, 466–470.

Tobie, G., Lunine, J.I., Sotin, C., 2006. Episodic outgassing as the origin of atmospheric methane on Titan. Nature, 440, 61–64.

Tomasko, M.G., Archinal, B., Becker, T., Bezard, B., Bushroe, M., Combes, M., Cook, D., Coustenis, A., de Bergh, C., Dafoe, L.E., Doose, L., Doute, S., Eibl, A., Engel, S., Gleim, F., Greiger, B., Holso, K., Howington-Kraus, E., Karkoschka, E., Keller, H.U., Kirk, R., Kramm, R., Kuppers, M., Lanagan, P., Lellouch, E., Lemmon, M., Lunine, J., McFarlane, E., Moores, J., Prout, G.M., Rizk, B., Rosiek,

M., Rueffler, P., Schroder, S.E., Schmitt, B., See, C., Smith, P., Soderblom, L., Thomas, N., West, R., 2005. Rain, wind and haze during the Huygens probe's decent to Titan's surface. Nature 438, 765–778.

Wilson, E.H., Atreya, S.K., 2004. Current state of modelling the photochemistry of Titan's mutually dependent atmosphere and ionosphere. J. Geophys. Res. 109, E06002.

Wong, A.-S., Morgan, C.G., Yung, Y.L., 2002. Evolution of CO in Titan. Icarus 155, 382–392.

Yelle, R.V., Strobel, D.F., Lellouch, E., Gautier, D. (1997). Engineering models for Titan's atmosphere. In: Lebreton, J.-P. (Ed.), Huygens: Science, Payload and Mission, ESA SP vol. 1177. ESA Publications Division, ESTEC, Noordwijk, The Netherlands, pp. 243–256.

Yung, Y.L., Allen, M., Pinto, J.P., 1984. Photochemistry of the atmosphere of Titan: comparison between model and observations. Astrophys. J. Suppl. 55, 465–506.